Relativistic reversal of the ponderomotive force in a standing laser wave

A. L. Pokrovsky and A. E. Kaplan*
Electrical and Computer Engineering Department, The Johns Hopkins University, Baltimore, Maryland 21218, USA
(Received 1 August 2005; published 11 October 2005; publisher error corrected 12 October 2005)

Effect of relativistic reversal of the ponderomotive force (PF), reported earlier for a collinear configuration of electron and laser standing wave [A. E. Kaplan and A. L. Pokrovsky, Phys. Rev. Lett., **95**, 053601 (2005)], is studied here theoretically for various types of polarizations of the laser beam. We demonstrated that the collinear configuration, in which the laser wave is linearly polarized with electric field $\vec{E}$ parallel to the initial electron momentum $\vec{p}_0$, is the optimal configuration for the relativistic reversal. In that case, the transverse PF reverses its direction when the incident momentum is $p_0=mc$. The reversal effect vanishes in the cases of circular and linear with $\vec{E}\perp\vec{p}_0$ polarizations. We have discovered, however, that the counter-rotating circularly polarized standing waves develop attraction and repulsion areas along the axis of laser, in the laser field whose intensity is homogeneous in that axis, i.e., has no field gradient.

DOI: 10.1103/PhysRevA.72.043401 PACS number(s): 42.50.Vk, 34.80.Qb, 61.14.−x, 42.65.Ky

I. INTRODUCTION

This work is a theoretical extension of our recent Letter [1] on fully relativistic ponderomotive force acting upon electrons in a standing laser wave. Ponderomotive (field-gradient) force (PF) is time-averaged (over a laser cycle) force acting on a charged particle in a spatially inhomogeneous electromagnetic (EM) field [2–5]. In the nonrelativistic regime this force always pushes the particles away from high-field areas and into the low-field areas. Conventional approach to handle the PF relies on adiabatic approximation, whereby one separates "slow" and "fast" motion to obtain a time-independent "ponderomotive potential" for the "slow" motion proportional to the field intensity $U(\vec{r})\propto|E(\vec{r})|^2$ and the PF, $\vec{F}_P=-\nabla U(\vec{r})$ [6,7]. For atoms and ions this force has a non-relativistic nature. However, in application to electrons, with advent of laser technology, PF can enter a strongly relativistic domain, where the laser field may readily exceed a relativistic scale $E_{\mathrm{rel}}=kmc^2/e$, whereby an electron is accelerated to relativistic energies within a laser half-cycle; here m is the rest mass of electron, and $k=\omega/c$ and ω are laser wave number and frequency. For lasers with the wavelength $\lambda=1$ μm the relativistic domain for electrons starts at the fields $E_{\mathrm{rel}}\approx 3.2\times 10^{10}$ V/cm or intensities $\approx 1.4\times 10^{18}$ W/cm^2. There are many applications and manifestations of PF, such as laser trapping and cooling of atoms [8–11], high-field photoionization of atoms [12,13], Kapitza-Dirac (KD) effect in a standing electromagnetic wave [14–17], plasmas and solids irradiated by powerful lasers [18,19], as well as observation of relativistic hysteretic resonances [20,21] and nonlinear optics of a single electron [22–25]. In-depth understanding of the PF in a traveling wave owes to the fact that the single electron motion in a plane electromagnetic wave is exactly solvable [26–30]. In a standing wave (SW), which, in fact, is the most fundamental configuration for the PF because of high field-gradient between the SW nodes, the PF was mainly studied via computer simulations in relation with transition to chaos and stochastic heating of electrons [31,32]. While original KD effect [14–17] assumed the use of a mirror to develop a standing wave, the superintense fields required for the experiments in relativistic regime, rule out such an arrangement. Most recent experiment [33], however, demonstrated feasibility of no-mirror generation of counterpropagating waves with the intensities higher than a few terrawatts. It should also be noted that some configurations with counterpropagating waves do not form a standing wave with nodes and antinodes (see below, Sec. IV B) and thus cannot be constructed by using reflection from a mirror.

In our Letter [1] we have developed an analytical theory of relativistic PF in a highly controllable and experimentally verifiable KD situation whereby an electron with sufficiently high incident momentum $\vec{p}_0$ is launched into a SW formed by two counterpropagating linearly polarized laser (L) beams. Electrons were considered to be launched from outside of the SW normally to its axis, along the direction of electric (E) field (collinear configuration). Here we provide a detailed derivation of the major results of Ref. [1], and generalization of the theory on circular and cross-linear (electric field perpendicular to $\vec{p}_0$) polarizations. Our analytical solutions allowed us to separate the PF into longitudinal (directed along the SW phase planes) and transverse components. This separation provides a clear physical picture of stability regions for electron trajectories. Theoretical results are verified by numerical simulations.

The paper is structured as follows. In Sec. II we formulate the problem and introduce the model and its parameters. Section III is devoted to the collinear electron-laser configuration. In the first part of it (Sec. III A) we consider an electron launched in an antinode plane of a linearly polarized SW with electric filed parallel to the initial momentum of electron. We show that there is a single parameter of the problem, which identifies the region of elastic electron scattering by the SW. We show the existence of adiabatic invariant, and find and analyze characteristics of motion. In the case of electrons launched along arbitrary SW plane, the magnetic

*Electronic address: sasha@striky.ece.jhu.edu

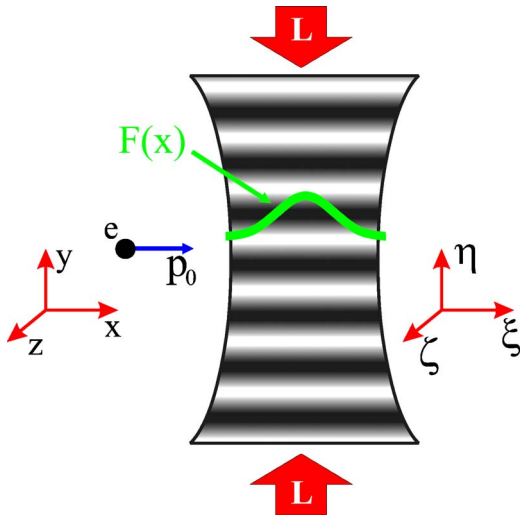

FIG. 1. (Color online) Configuration of electron and the standing wave. $F(x)$ is a profile of the laser beam, p_0 is the initial electron momentum.

(M) laser field becomes a significant player and brings about a rich landscape of motion patterns. This general case is treated in Sec. III B. Our major discovery is that in addition to a large KD effect (considered in Sec. III C), the PF in the direction normal to the incident momentum, exhibits a dramatic sign reversal with a relativistic threshold: while remaining high-field repelling along $\vec{p}_0$, PF normal to $\vec{p}_0$ reverses into high-field attractive force, if $p_0 > mc$. In Sec. IV we study all other (noncollinear) configurations of SW and investigate the existence of the switching effect in these cases.

II. BASIC MODEL

We consider two weakly focused Gaussian L beams with the spatial profile $F(x)$ vanishing in the wings $[F(x) \to 0$ as $|x| \to \infty]$, counterpropagating, and forming a SW in the y axis, and an electron launched in the transverse x axis near their focal plane (Fig. 1). To study and analyze the electron motion in the field of the SW we use relativistic Lorentz equation

$$\frac{d\vec{p}}{dt} = e\vec{E} + \frac{e}{mc}\frac{\vec{p}}{\gamma} \times \vec{H}, \tag{1}$$

$$\frac{d\vec{r}}{dt} = \vec{v} = \frac{\vec{p}}{m\gamma}, \tag{2}$$

where $\gamma = \sqrt{1 + (p/mc)^2}$ is the relativistic factor, $\vec{E}$ and $\vec{H}$ are electric and magnetic fields of the SW, respectively, $\vec{v}$ is electron velocity, and $\vec{r}$ is position vector of electron. To concentrate on the significant features of the phenomenon, we assume "slab" two-dimensional (2D) beams stretched in the z axis, i.e., $\partial F/\partial z = 0$.

In our calculations here we neglected the radiation "friction," or self-action force on the electron. Our estimates and numerical simulations showed it is negligible for the specific situation. Indeed, the time of the electron passing through the laser beam is relatively short, and for the radiation friction to affect the motion, one needs $\gamma = O(10^3)$, which is far beyond the domain of interest, see also Refs. [22–24]. As far as the laser-electron interaction, we used strictly classical approach, since in the cases of interest, a typical number of photons exchanged between an electron and laser per cycle exceeds $\sim mc^2/\hbar\omega = O(10^6)$, and quantum dispersion $\Delta_q = \langle \Delta N \rangle / N$ is much smaller than a small parameter of the problem μ_ξ, i.e., $\Delta_q = (N_{\rm ph})^{-1/2} \ll \mu_\xi$ [see Eq. (11) below]. In our calculations we use normalized coordinates

$$\xi = xk, \quad \eta = yk, \quad \zeta = zk, \tag{3}$$

time $\tau = \omega t$, momentum $\vec{\rho} = \vec{p}/mc$, $\gamma = \sqrt{1 + \rho^2}$, and amplitude profile $f(\xi) = F/E_{\rm rel}$. To verify theoretical results we have performed numerical simulations, whereby equations of motion were integrated with no *a priori* assumptions about the nature of the electron motion. In most of realistic laser beams, the laser amplitude/intensity profile in their cross sections can be assumed to have Gaussian shape. However, since any numerical simulation has to use finite size of an L beam, to assure reliability of the simulation, it is more appropriate to assume an amplitude profile that zeroes out at the "edges" of the L beam and is smooth everywhere including those edges, i.e., has at least its first derivative zeroing out at those points. All the figures in this paper are results of calculations with such a model laser profile taken in a Gaussian-like form

$$f(\xi) = \begin{cases} f_{\rm pk} \cos^2 \dfrac{\xi}{\xi_L} & \text{at } |\xi| < \dfrac{\pi \xi_L}{2}, \\ 0 & \text{otherwise}, \end{cases} \tag{4}$$

that satisfy the above conditions; here ξ_L is roughly half-size of the beam profile. Initial conditions for electron are

$$\vec{p} = p_0 \hat{e}_\xi \text{ and } \xi = -\frac{\pi \xi_L}{2} \text{ at } \tau = 0. \tag{5}$$

This choice of the profile was found to be optimal for our numerical calculations. We also checked that qualitatively, all the results hold for the Gaussian profile. Note that all the analytical results are valid for arbitrary profile function $f(\xi)$ (subject only to a condition imposed on its gradient; see explanations below in Sec. III A) and they are not limited neither by Gaussian shape nor by the model (4).

III. COLLINEAR POLARIZATION OF THE FIELD-ELECTRON SYSTEM

Our calculations showed that some of the most interesting effects are brought about by the specific configuration of the field as related to the electron momentum. Specifically, it is the case, when both counterpropagating waves in the SW are linearly polarized along the same line as the incident momentum of an electron. In this case, we write the electric field of the SW as $\vec{E}/E_{\rm rel} = \hat{e}_\xi f(\xi) \cos \eta \sin \tau$, and the Lorentz equations take the form

$$\frac{d\rho_\xi}{d\tau} = f(\xi) \cos \eta \sin \tau + \frac{\rho_\eta}{\gamma} f(\xi) \sin \eta \cos \tau, \tag{6}$$

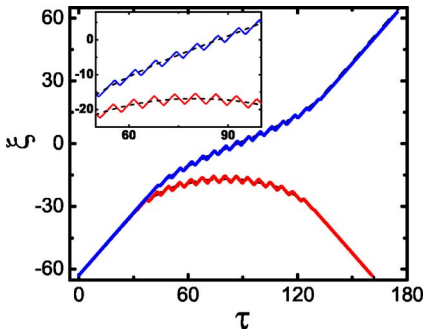

FIG. 2. (Color online) Typical motions of electrons passing through (upper curve) and reflected from (lower curve) the antinode of laser SW ($f_{\mathrm{pk}}=15$, $\xi_L=40$). Here $\rho_0=11$ and 8, respectively, with the threshold $\rho_{\mathrm{thr}}\approx 9.59$. Solid lines: the full motion ξ, dashed lines: time-averaged $\tilde{\xi}$. The inset depicts an enlarged center region of the main plot.

$$\frac{d\rho_\eta}{d\tau}=-\frac{\rho_\xi}{\gamma}f(\xi)\sin\,\eta\cos\,\tau, \tag{7}$$

$$\frac{d\xi}{d\tau}=\frac{\rho_\xi}{\gamma},\quad \frac{d\eta}{d\tau}=\frac{\rho_\eta}{\gamma}. \tag{8}$$

These equations allow one to consider electrons launched in arbitrary plane of the SW. However, the case, when electron is launched in an antinode plane is very special since it allows for the most comprehensive analytical treatment, and we will consider it first in Sec. III A.

A. Electron motion in antinode plane

Thus, we start with the case of electron launched in an antinode plane $\eta=n\pi$ (n is an integer number), where the E field has spatial maximum along the axis of the L beam, and the M field vanishes. Allowing for thorough analytical treatment, this case makes a good reference point. More importantly, those planes become strong attractors for relativistic trajectories, see below Sec. III B. Equations (6)–(8) are then reduced to

$$\frac{d\rho}{d\tau}=f(\xi)\sin\,\tau,\quad \frac{d\xi}{d\tau}=\frac{\rho}{\gamma}, \tag{9}$$

where $\rho\equiv\rho_\xi$. As usual, we choose the field gradient $df/d\xi$ sufficiently small. Characterizing the field gradient by the scale of transverse inhomogeneity in the laser beam ξ_L and assuming that the motion of an electron can always be presented as "slow" motion, indicated by the tilde and small "fast" oscillations $\delta\xi$ of the coordinate ξ with the laser frequency, we will stipulate that the amplitude of the fast oscillations is small enough compared to the scale ξ_L. Writing the full motion of electron as $\xi\approx\tilde{\xi}+\delta\xi$, where

$$\overline{\delta\xi}\equiv\int_0^{2\pi}\delta\xi(\tau)d\tau=0, \tag{10}$$

with the overbar designating averaging over the oscillation period, one can show by direct calculations that for an arbitrary relativistic case, we have $|\delta\xi|\leqslant\pi/2$. Indeed, the limiting speed of electron is the speed of light, $|\beta|\equiv|\vec{v}|/c=1$, so that within a laser cycle the full swing of electron is $\sim\pi$, and the maximum amplitude of the swing is $\pi/2$. In the case of relativistic field, $f^2\gg 1$, we can write $\beta\approx\mathrm{sgn}(\rho)$, and because of that, the electron trajectory, $\xi(\tau)$, assumes a sawtooth shape, see Fig. 2.

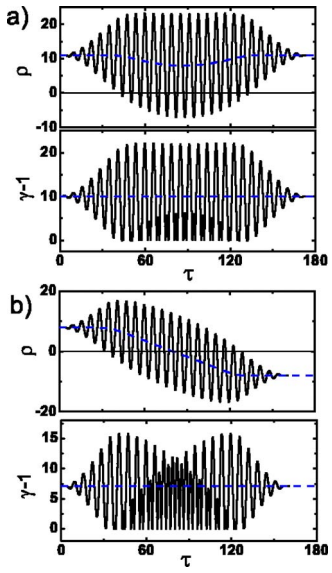

FIG. 3. (Color online) Fast oscillations of dimensionless energy $\gamma-1$ and momentum ρ of electrons passing through (a) and reflected from (b) the laser beam (the parameters are the same as in Fig. 2). The dashed lines are evolutions of the "slow" components $\tilde{\gamma}$, $\tilde{\rho}$ obtained as the numerical solution of Eq. (16).

The condition of laser ξ-profile smoothness is

$$\xi_L\gg\xi_{\mathrm{osc}}\equiv\min\left(\frac{\pi}{2},f_{\mathrm{pk}}\right)\ \text{or}\ \mu_\xi\equiv\frac{\xi_{\mathrm{osc}}}{\xi_L}\ll 1, \tag{11}$$

where f_{pk} is the peak magnitude of the amplitude profile and μ_ξ is the small parameter. This condition is sufficient for the system to exhibit elastic scattering, including the strongly relativistic case, whereby the fast oscillations of momentum and energy may be large when the laser amplitude f_{pk} is high, see Fig 3. Using Eq. (11), and writing the laser profile f viewed by an electron as

$$f(\xi)=f(\tilde{\xi})+\frac{df}{d\tilde{\xi}}\delta\xi+\mu_\xi\mathrm{O}\left[\frac{df}{d\tilde{\xi}}\delta\xi\right]. \tag{12}$$

we have from the first equation of Eq. (9) that

$$\rho\approx\tilde{\rho}-f(\tilde{\xi})\cos\,\tau+\mu_\xi\mathrm{O}[f(\tilde{\xi})]. \tag{13}$$

Writing a Fourier series for $\delta\xi$ as

$$\delta\xi=\xi_1\sin\,\tau+\xi_{1c}\cos\,\tau+\xi_2\sin(2\tau+\psi_2)+\cdots \tag{14}$$

one can show that only the first term in Eq. (14) is significant for the "slow" motion, even when $\delta\xi(\tau)$ has a relativistic, sawtooth shape, so to proceed, we can write

$$\xi \approx \tilde{\xi} + \xi_1 \sin\tau, \quad \rho \approx \tilde{\rho} - f(\tilde{\xi})\cos\tau. \tag{15}$$

Substituting this into Eq. (9), we have now adiabatic equations for "slow" motion alone as

$$\frac{d\tilde{\rho}}{d\tau} = \frac{1}{2}\frac{df(\tilde{\xi})}{d\tilde{\xi}}\xi_1[\tilde{\rho}, f(\tilde{\xi})], \quad \frac{d\tilde{\xi}}{d\tau} = \tilde{\beta}[\tilde{\rho}, f(\tilde{\xi})], \tag{16}$$

where

$$\tilde{\beta} = \frac{1}{2\pi}\int_0^{2\pi} \frac{\tilde{\rho} - f(\tilde{\xi})\cos\tau}{\sqrt{1 + [\tilde{\rho} - f(\tilde{\xi})\cos\tau]^2}} d\tau, \tag{17}$$

$$\xi_1 = \frac{1}{\pi}\int_0^{2\pi} \frac{[\tilde{\rho} - f(\tilde{\xi})\cos\tau]\cos\tau}{\sqrt{1 + [\tilde{\rho} - f(\tilde{\xi})\cos\tau]^2}} d\tau. \tag{18}$$

Using the relativistic factor of an electron, i.e., dimensionless energy γ we introduce now its averaging over the laser period, $H \equiv \tilde{\gamma}$, i.e., "slow" energy as

$$H(\tilde{\rho}, \tilde{\xi}) = \frac{1}{2\pi}\int_0^{2\pi} \sqrt{1 + [\tilde{\rho} - f(\tilde{\xi})\cos\tau]^2} d\tau \tag{19}$$

(note that in general $H = \tilde{\gamma} \neq \sqrt{1 + \tilde{\rho}^2}$ and $\tilde{\rho} \neq \tilde{\beta}\tilde{\gamma}$!). It is then readily verified that Eq. (16) can now be written in the canonical Hamiltonian form as

$$\frac{d\tilde{\rho}}{d\tau} = -\frac{\partial[H(\tilde{\rho}, \tilde{\xi})]}{\partial\tilde{\xi}}, \quad \frac{d\tilde{\xi}}{d\tau} = \frac{\partial[H(\tilde{\rho}, \tilde{\xi})]}{\partial\tilde{\rho}} \tag{20}$$

from which it transpires that $H(\tilde{\rho}, \tilde{\xi})$ is the (adiabatic) Hamiltonian, and thus is to be conserved during the motion. Indeed, evaluating the time derivative of H

$$\frac{dH}{d\tau} = \frac{\partial H}{\partial\tilde{\rho}}\frac{d\tilde{\rho}}{d\tau} + \frac{\partial H}{\partial\tilde{\xi}}\frac{d\tilde{\xi}}{d\tau} = 0, \tag{21}$$

we can see that H is the invariant of motion: $H = inv = \gamma_0$, where γ_0 is the relativistic factor of incident electron. The same result is obtained by assuming an arbitrary phase ϕ of the laser field, i.e., by replacing τ in Eq. (9) by $\tau + \phi$. If we have an incoherent electron beam with electrons arriving randomly, time averaging in all calculations can be replaced by averaging over the ensemble of all the phases $0 \leqslant \phi < 2\pi$; by designating it with angular brackets, we arrive at the same result, i.e., the system has an *ergodicity* property

$$\langle\xi\rangle = \tilde{\xi}, \quad \langle\rho\rangle = \tilde{\rho}, \quad \langle\beta\rangle = \tilde{\beta} \tag{22}$$

and

$$H(\tilde{\rho}, \tilde{\xi}) = \tilde{\gamma} = \langle\gamma\rangle = inv = \gamma_0. \tag{23}$$

One can view Eq. (23) as conservation of a full adiabatic relativistic energy. Elegantly simple, this result in hindside may seem to be almost obvious, but this is not quite the case. On the surface of it, H is a legitimate "full energy," but the adiabatic nature of this Hamiltonian makes it one of those rare cases where it cannot be split into kinetic and potential energies nor into polynomial form, except for the nonrelativistic case, see below. Interpretations aside, this creates a tough problem, e.g., when one tries to develop quantum mechanics of "slow" relativistic motion by replacing the Hamiltonian (19) with the set of regular operators. The situation here is reminiscent of the physics of strongly nonlocal processes. While nonadiabatic relativistic energy γmc^2 still allows for procedure resulting in Dirac equation for a wavefunction, the averaging in Eq. (19) makes this problematic, especially in the strongly relativistic case of violently huge nonlinear oscillations of both momentum and energy during the laser cycle, see Fig. 3. In view of those processes, it is in fact amazing that the invariant of motion (23) holds; there is no way of knowing *a priori* that the "potential" energy due to laser field will not come into play separately from γ, which is usually associated with kinetic energy.

Let us consider a few characteristic or limiting cases.

(a) For arbitrary momentum ρ but nonrelativistic EM field $f^2 \ll 1$, Eq. (23) yields

$$\sqrt{1 + \tilde{\rho}^2} + \frac{f^2(\tilde{\xi})}{4(1 + \tilde{\rho}^2)^{3/2}} = inv = \gamma_0. \tag{24}$$

(b) In particular, in the fully nonrelativistic case ($\rho^2, f^2 \ll 1$) one has as expected:

$$\frac{\tilde{\rho}^2}{2} + U(\tilde{\xi}) = inv = \frac{\rho_0^2}{2}, \tag{25}$$

where $\tilde{\rho}^2/2$ is slow kinetic energy, and $U(\tilde{\xi}) = f^2(\tilde{\xi})/4$ is an effective potential. This is the only case when the kinetic and potential energies of slow motion can be separated.

(c) The case of the strongly relativistic EM field, $f(\xi)^2 \gg 1$. Based on the approximation whereby, due to Eq. (15), during most of the oscillation period $\gamma \approx |\tilde{\rho} - f(\tilde{\xi})\cos\tau|$, Eqs. (19) and (23) yield

$$\tilde{\rho}\sin^{-1}\left[\frac{\tilde{\rho}}{f(\tilde{\xi})}\right] + \sqrt{f^2(\tilde{\xi}) - \tilde{\rho}^2} = inv = \pi\rho_0/2, \tag{26}$$

if $\tilde{\rho}^2/f^2 \leqslant 1$, and $\tilde{\rho}^2 \approx \rho_0^2$ otherwise; no specific terms can be assigned here to either kinetic or potential energies.

(d) A turning point $\tilde{\xi}_{\mathrm{trn}}$ at which the electron slow trajectory comes to a complete stop, i.e., $\tilde{\rho} = 0$, is determined by the relationship $H(0, \tilde{\xi}_{\mathrm{trn}}) = \gamma_0$ or

$$\frac{2\sqrt{1 + f^2(\tilde{\xi}_{\mathrm{trn}})}}{\pi} E\left[\frac{f(\tilde{\xi}_{\mathrm{trn}})}{\sqrt{1 + f^2(\tilde{\xi}_{\mathrm{trn}})}}\right] = \gamma_0, \tag{27}$$

where $E(u)$ is a complete elliptic integral of the second kind [34].

(e) Of special interest is a threshold incident energy γ_{thr}, marking the switch from full reflection ($\rho_{\mathrm{out}} = -\rho_0$) to full transmission ($\rho_{\mathrm{out}} = \rho_0$). This case corresponds to the turning point coinciding with the peak amplitude of the EM-field profile f_{pk}; hence

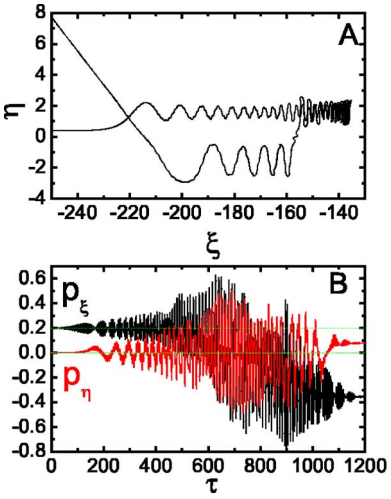

FIG. 4. (Color online) Trajectory (A) and momenta (B) of electron normally incident on a SW in the collinear configuration (linearly polarized L beam with $\vec{E}\|\vec{p}_0$) at $\eta_0=\pi/8$ with initial momentum $\rho_0=0.2$ ($f_{pk}=2.0, \xi_L=160$).

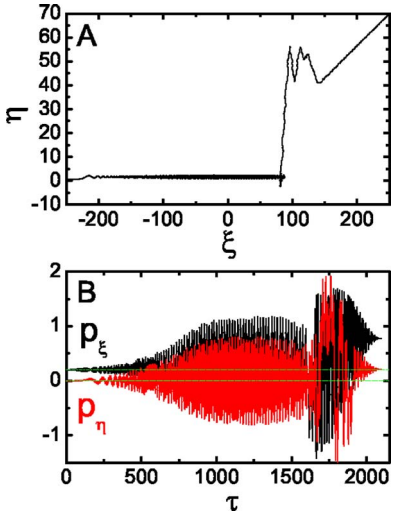

FIG. 5. (Color online) Trajectory (A) and momenta (B) of electron normally incident on a SW in the collinear configuration at $\eta_0=\pi/5$ with initial momentum $\rho_0=0.2$ ($f_{pk}=2.0, \xi_L=160$).

$$\gamma_{thr}=\frac{2\sqrt{1+f_{pk}^2}}{\pi}E\left[\frac{f_{pk}}{\sqrt{1+f_{pk}^2}}\right]. \tag{28}$$

Amazingly, the threshold incident momentum, $\rho_{thr}=\sqrt{\gamma_{thr}^2-1}$ vs f_{pk} is an almost linear function. In both nonrelativistic ($f_{pk}^2\ll 1$) and high-relativistic ($f_{pk}^2\gg 1$) limits we have $\rho_{thr}=af_{pk}$, where $a=1/\sqrt{2}$ and $a=2/\pi$, respectively, i.e., a does not change drastically. In the entire range of f_{pk}, a good interpolation with the precision better than 1% everywhere holds:

$$\rho_{thr}\approx\frac{f_{pk}}{\sqrt{2}}\sqrt{\frac{A+8f_{pk}^2}{A+\pi^2 f_{pk}^2}}, \tag{29}$$

where $A=16(\pi^2-8)\sim 30$.

The scattering due to adiabatic motion here is fully elastic; whether passing through the laser beam or being reflected from it, an electron comes out with the same, incident energy, i.e., $\gamma_{out}=\gamma_0$, whereas its momentum is conserved only if the electron passes through $\rho_{out}=\rho_0$. Otherwise, it reverses its sign, $\rho_{out}=-\rho_0$ (Fig. 3), while the deficit momentum $2\rho_0$ is absorbed by the laser beam, which should result in the beam's slight deflection. However, when the adiabatic condition (11) is violated, i.e., the field gradient is not small enough, the relativistic field and electrons may exhibit large nonelastic scattering resulting in particular in dramatic energy transfer from laser to electrons that may allow for multi-MeV acceleration of electrons per pass and very tight focusing of electrons after they pass through the laser beam. These effects will be addressed by us elsewhere.

B. Arbitrary plane of incidence

In the previous section we considered electron motion along the antinode plane, where the M field is zero. Now let us study the general case of arbitrary incidence, whereby an electron is launched into a SW in an arbitrary plane that thus has a nonvanishing M field. In the nonrelativistic case, the M field [second term in the right-hand side of Eq. (1)] for many purposes can be ignored since $\rho\ll 1$. In linearly polarized traveling wave for $\rho\gg 1$ [26] it results in "8-like" trajectories. Standing wave opens a whole new can of worms: oscillation "channeling" of electrons, "sneaky" transmission modes, huge KD-effect in transmission and reflection, etc.; but most of all—relativistic reversal of PF.

For the motion normal to the SW planes, the fundamental fact that rules out general adiabatic theory is that at $\gamma\gg 1$ the full swing of fast oscillations across the SW planes may reach $\lambda/2$, which is precisely the spacing between adjacent SW planes. This disallows the assumption that the η-inhomogeneity scale can always be small, since $(\mu_\eta)_{max}=(\eta_{osc})_{max}/\pi=1$ [compare with Eq. (11)]. Numerical simulations [31,32] in most of the cases exhibit chaos. Typical electron behavior (trajectory and momenta) in the chaotic regime is shown in Figs. 4 and 5. Parameters of simulations for these figures are $f_{pk}=2$, $\xi_L=160$, $\rho_0=0.2$, and electron is launched into a standing wave at $\eta_0=\pi/8$ and $\eta_0=\pi/5$ for Fig. 4 (reflection) and 5 (transmission), respectively. One can see "channeling" in the electron trajectories, whereby electron oscillates near some phase plane of the SW during many laser cycles and then, at some point, jumps to another plane, or just streams away along the SW axis.

Here, however, we are interested in well-controlled electron motion that would enable us to predict and use new physical effects and determine their characteristics and areas of existence, in particular the accessibility and stability domains of the various modes (e.g., antinode modes). The main condition of interest to us here is the case whereby the electron momentum strongly dominates over the momentum due to the laser field, $\mu_L=f_{pk}/\rho_0\ll 1$. In such a case, the motion is adiabatic and can be well analyzed; note, that this condition does not preclude momentum ρ_0 and field f_{pk} becoming strongly relativistic. We separate again slow and fast electron motion (similarly to the procedure described in Sec. III A), and the small parameters of electron motion are $(\delta\xi)_{max}$

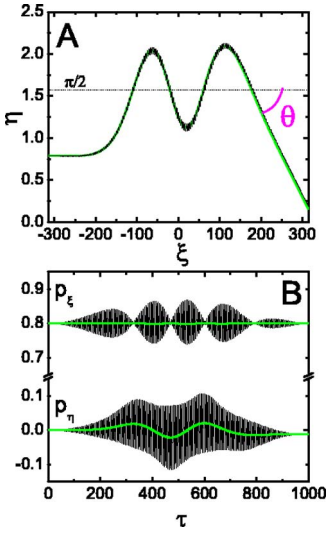

FIG. 6. (Color online) Trajectory (A) and momenta (B) of electron normally incident on a SW in the collinear configuration at $\eta_0=\pi/4$ with initial momentum below the switching threshold ($\rho_0=0.8$, $f_{\rm pk}=0.1$, $\xi_L=200$).

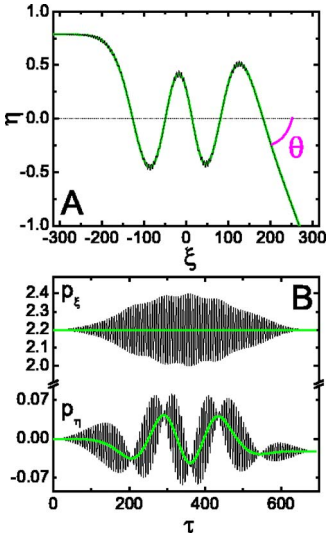

FIG. 7. (Color online) Trajectory (A) and momenta (B) of electron normally incident on a linearly polarized L beam with $\vec{E}\|\vec{p}_0$ at $\eta_0=\pi/4$ with initial momentum above the switching threshold ($\rho_0=2.2$, $f_{\rm pk}=0.2$, $\xi_L=200$).

$\equiv\mu_\xi=O(\xi_L^{-1})\ll 1$ and $(\delta\eta)_{\max}=\mu_L\ll 1$, where $\delta\xi$ and $\delta\eta$ are the amplitudes of fast ξ and η oscillations. We seek for a solution in the following form, keeping slow motion and the first order harmonics only:

$$\xi\approx\tilde{\xi}+\xi^c\cos\tau+\xi^s\sin\tau, \tag{30}$$

$$\eta\approx\tilde{\eta}+\eta^c\cos\tau+\eta^s\sin\tau, \tag{31}$$

$$\rho_\xi\approx\tilde{\rho}_\xi+\rho_\xi^c\cos\tau+\rho_\xi^s\sin\tau, \tag{32}$$

$$\rho_\eta\approx\tilde{\rho}_\eta+\rho_\eta^c\cos\tau+\rho_\eta^s\sin\tau, \tag{33}$$

where superscripts "c" and "s" label the slow-varying coefficients (to be evaluated later on) in terms with fast-varying functions $\cos\tau$ and $\sin\tau$, respectively; these notations will be used by us throughout the rest of this paper. Substituting Eqs. (30)–(33) into Eqs. (6)–(8) and evaluating coefficients for each harmonic separately one can obtain the amplitudes of fast oscillations and the equation of "slow" motion. Keeping only the leading terms with respect to the small parameters μ_L and μ_ξ, the result is

$$\rho_\xi^c=-f(\beta_0\tau)\cos\tilde{\eta},\quad \rho_\xi^s=\frac{f(\beta_0\tau)}{\tilde{\gamma}}\tilde{\rho}_\eta\sin\tilde{\eta}, \tag{34}$$

$$\rho_\eta^c=0,\quad \rho_\eta^s=-\frac{f(\beta_0\tau)}{\tilde{\gamma}}\rho_0\sin\tilde{\eta}, \tag{35}$$

$$\xi^c=-\frac{f(\beta_0\tau)}{\tilde{\gamma}^4}\tilde{\rho}_\eta\sin\tilde{\eta},\quad \xi^s=-\frac{f(\beta_0\tau)}{\tilde{\gamma}^3}\cos\tilde{\eta}, \tag{36}$$

$$\eta^c=\frac{f(\beta_0\tau)}{\tilde{\gamma}^2}\rho_0\sin\tilde{\eta},\quad \eta^s=0, \tag{37}$$

and the equations of slow motion are

$$\tilde{\xi}=\beta_0\tau,\quad \tilde{\rho}_\xi=\rho_0, \tag{38}$$

$$\frac{d\tilde{\rho}_\eta}{d\tau}=\frac{f^2(\beta_0\tau)}{4\tilde{\gamma}^3}(1-\rho_0^2)\sin(2\tilde{\eta}),\quad \frac{d\tilde{\eta}}{d\tau}=\frac{\tilde{\rho}_\eta}{\tilde{\gamma}}, \tag{39}$$

where $\tilde{\gamma}=\gamma_0=\sqrt{1+\rho_0^2}$. Equation (39) can be rewritten as a second order differential equation for slow variable $\tilde{\eta}$:

$$\frac{d^2\tilde{\eta}}{d\tau^2}+f^2(\beta_0\tau)\frac{\rho_0^2-1}{4\gamma_0^4}\sin(2\tilde{\eta})=0,\quad \tilde{\rho}_\eta=\gamma_0\frac{d\tilde{\eta}}{d\tau}, \tag{40}$$

i.e., the η oscillations are pendulumlike. Their small-oscillation slowly varying frequency is

$$\Omega_\eta(\tau)=f(\beta_0\tau)\frac{\sqrt{|\rho_0^2-1|}}{\sqrt{2}\gamma_0^2} \tag{41}$$

and it reaches its maximum in the middle of the L beam, where $f=f_{\rm pk}$. The equilibrium points of Eq. (40) are $\eta=\pm n\pi/2$; each stable point (focus) is alternated by an unstable point (saddle).

The most remarkable feature of Eq. (40) is that at a certain switching point $\rho_0^2=1$ (or $p_0=mc$), slow oscillations vanish, while the stable and unstable points of Eq. (40) reverse their positions. At $\rho_0^2<1$, the stable points are $\eta=(n+1/2)\pi$, hence the planes of attraction for the trajectories are the nodes, see Fig. 6(a), i.e., the planes of the maximum M field (and zero E field) of the SW wave (the points $\eta=n\pi$ are unstable, saddle, points). Slow oscillating solid lines for $\tilde{\eta}$ in Fig. 6(a) and for $\tilde{\rho}_\eta(\tau)$ in Figs. 6(a) and 6(b), obtained directly from numerical solution of Eq. (40), coincide within the line thickness with the cycle averaging of the full motion.

However, in the relativistic area, at $\rho_0^2>1$, the points $\eta=n\pi$ become stable, Fig. 7(a), and the antinodes considered in detail in the first part of the paper, become the plane of attraction, whereas $\eta=(n+1/2)\pi$ correspond to saddle

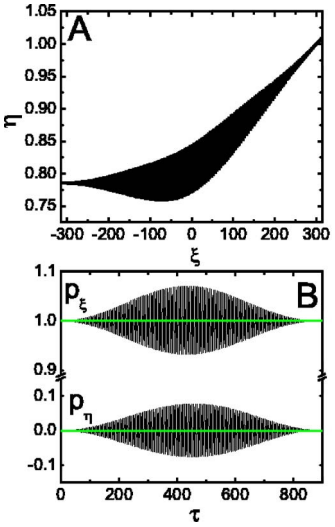

FIG. 8. (Color online) Trajectory (A) and momenta (B) of electron normally incident on a linearly polarized L beam with $\vec{E}\|\vec{p}_0$ at $\eta_0=\pi/4$ with initial momentum equal to the switching threshold ($\rho_0=1.0$, $f_{\rm pk}=0.1$, $\xi_L=200$).

points. At $\rho_0^2=1$, we have $\Omega_\eta=0$, Fig. 8. Thus, the ponderomotive force reverses its direction at $\rho_0^2=1$ or $p_0=mc$. In fact, it is the only effect that we know of that pins down a clear borderline between "relativistic" and "nonrelativistic" motions. This borderline corresponds to $\gamma_0=\sqrt{2}$, or ~212 KeV electron kinetic energy, which can readily be accessed by using an electron microscope. In the non-relativistic limit Eq. (40) reduces to a regular η-gradient-force equation with $\rho_0 \ll 1$ and $\gamma_0 \approx 1$, and nodes $\tilde{\eta}=(n+1/2)\pi$ being stable points. One can show, that in case when the SW is linearly polarized with electric field making a small angle $\theta_E \ll 1$ with the direction of initial momentum $\vec{p}_0$, the switching of stable and unstable equilibrium points occurs at $\rho_0=1+O[\theta_E^2]$.

The PF reversal effect here can be explained this way. The PF normal to the E polarization and $\vec{\rho}_0$ is induced by the second, "magnetic" term on the right-hand side of Eq. (1), proportional to γ^{-1}. Fast oscillations of γ (such as, e.g., in Refs. [22–25]) create the force counteracting to the "regular," nonrelativistic, PF. That new force is getting dominant at $\rho_0 \gg 1$. At $\rho_0=1$, these two nearly cancel each other. [In the one-dimensional (1D) case, Eq. (9), the magnetic term is absent.]

C. Trajectory and frequency of the slow motion; Kapitza-Dirac effect

Equation (40) also describes trajectory $\tilde{\eta}(\tilde{\xi})$ if τ is replaced with $\tilde{\xi}/\beta_0$, so that

$$\frac{d^2\tilde{\eta}}{d\tilde{\xi}^2}+f^2(\tilde{\xi})\frac{\rho_0^2-1}{(2\rho_0\gamma_0)^2}\sin(2\tilde{\eta})=0. \tag{42}$$

If an electron makes a few η oscillations, i.e., if $(\Omega_\eta)_{\rm pk}\xi_L/\beta_0 \gg 1$, the small η oscillations with the launching point $\eta=\eta_0$, can be obtained from Eq. (40) via the WKB approximation as

$$\eta(\tau) \propto (\eta_0-\eta_{\rm st})\sqrt{\frac{f_{\rm pk}}{f(\beta_0\tau)}}\sin[\Phi(\tau)], \tag{43}$$

$$\Phi(\tau)=\int_{-\infty}^{\tau}\Omega_\eta(t)dt \gg 2\pi, \tag{44}$$

and $\eta_{\rm st}$ is a stable point nearest to η_0; it explains why the slow η oscillations are pinched down at the peak field. These oscillations can be observed via E-beam EM radiation with the low-frequency spectrum that has a cutoff frequency

$$\Omega_{\rm cut}=\frac{f_{\rm pk}}{\gamma_0^2}\sqrt{\frac{|\rho_0^2-1|}{2}}, \tag{45}$$

as well as via modulation of the laser frequency with respective frequencies, $\omega_{\rm scat}=\omega_L\pm\Omega_\eta$, i.e., self-scattering of laser at electrons in a quasiresonant SW system. The highest possible frequency for a given $f_{\rm pk}$ corresponds to $\rho_0=\sqrt{3}$, at which $(\Omega_{\rm cut})_{\rm max}=f_{\rm pk}/4$. Due to the η oscillations, when an electron approaches far outer edge of the L beam, it can be angularly deflected due to a "slingshot" effect, causing thus superstrong relativistic KD effect. The highest possible angle of deflection $\theta_{\rm max}\sim(\tilde{\rho}_\eta)_{\rm max}/\rho_0$ is estimated as

$$\theta_{\rm max}\sim\frac{\pi}{2^{3/2}}\frac{f_{\rm pk}}{\rho_0}\sqrt{\frac{|\rho_0^2-1|}{\gamma_0}} \tag{46}$$

or, if $\rho_0^2 \gg 1$, $\theta_{\rm max}\sim(\pi/2^{3/2})f_{\rm pk}/\rho_0$; e.g., for $\rho_0=2$ and $f_{\rm pk}=1/\sqrt{2}$, we have $\theta_{\rm max}\sim\pi/8$, a huge effect. This KD deflection for $\rho_0^2\neq 1$ is seen in Figs. 6 and 7 for $\tilde{\rho}_\eta$ and especially for $\tilde{\eta}$; it also exists even for $\rho_0^2=1$ because of the higher order corrections in μ_L and $\mu_{\tilde{\xi}}$, Fig. 8(a), but is too small to show up in the Fig. 8(b) for $\tilde{\rho}_\eta$.

Sufficient conditions to prevent the system from sliding into instability and chaos is that the incident momentum is strong enough compared to the E field, $\rho_0^2 \gg f_{\rm pk}^2$, or the L beam size, $2\xi_L$ is sufficiently short. In fact, strong chaos in SW in Refs. [31,32] was apparently facilitated by an electron being born inside the L beam and having low initial momentum, and L beam size being very large or infinite. For $\rho_0>1$, most "permissive," middle entrance point $\eta_0=\pi/4$, and sufficiently long run $\xi_L=200$ (50λ waist), we found that the stability area for $\rho_0>1$ is determined by a simple formula $\rho_0/f_{\rm pk}>{\rm const}\approx 2$.

The areas of parameters $f_{\rm pk}$, ρ_0, and η_0, where the system is still stable, exist even if $f_{\rm pk}^2 \gg \rho_0^2$ albeit they are relatively narrow. Of interest here are reflection modes; even if $f_{\rm pk}^2 \gg 1$, but ρ_0 is sufficiently small (typically, <0.07), the slow ξ motion may come to a complete stop similarly to Eq. (27) far before it reaches the point where $f_{\rm pk}$ peaks out, Fig. 9(b). For $f_{\rm pk}<2.3$, there are still areas of ρ_0 and η_0, where electrons with relatively low ρ_0 are still able to "sneak through," Fig. 9(a).

IV. NONCOLLINEAR LASER-ELECTRON CONFIGURATIONS

In the previous sections we discussed only collinear configuration, i.e., the case of linearly polarized L beams with

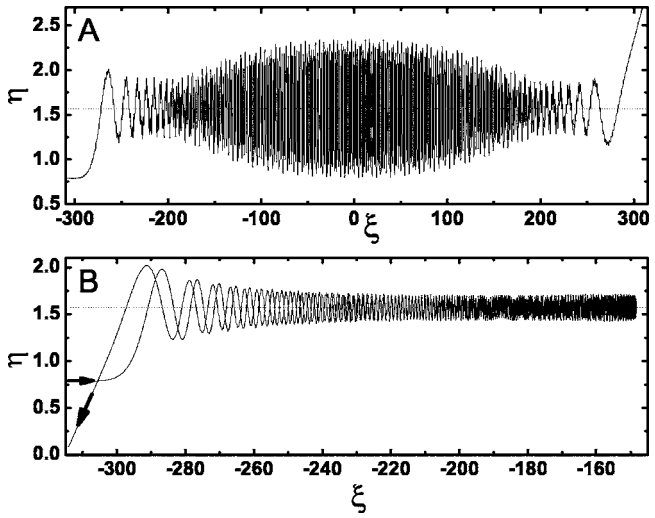

FIG. 9. Transmission (A) and reflection (B) trajectories of electron normally incident on a linearly polarized L beam with $\vec{E}\|\vec{p}_0$ ($f_{\mathrm{pk}}=2$, $\xi_L=200$) at $\eta_0=\pi/4$; $\rho_0=0.325$ (A), 0.06 (B).

electric field having only component along the initial electron momentum $\vec{p}_0$. Let us consider other polarizations while studying electron motion in the general case of an arbitrary plane of incidence. In general, there could be many possible configurations involving different mutual polarizations of both L beams, and different configurations between these polarizations and the direction of the momentum of incident electrons. For example, one can consider two L beams still collineraly polarized, but their polarization making a certain angle with the incident electron momentum; one can further consider that two L beams are still linearly polarized, but their polarizations are not parallel to each other; one of the L beams is linearly polarized, while another one is circularly polarized, etc. The most general case would be the one whereby the both L beams are elliptically polarized with the ellipses of their polarization having different ellipticity, different directions of their main axes, arbitrary direction of mutual rotation, and they make arbitrary angle with the incident electron momentum. However, for the sake of simplicity and briefness, in addition to the above considered collinear configuration, we will address here only three more configurations, which we consider to be the major ones. One of them is the case whereby two L beams are collinearly polarized, but their polarization is *normal* to the momentum of incident electron, and two other cases whereby both L beams are circularly polarized: one with those circular polarizations being corotating, and another one with them being counter-rotating. Each one has an interesting peculiarity.

As in Sec. III B, we will analyze the regime of strong electron momentum dominance $f_{\mathrm{pk}}/\rho_0 \ll 1$. We again chose a 2D L-beam profile, uniform in the z direction. However, for the polarizations studied in this section, electron motion is three dimensional. Major questions of interest are whether the reversal effect exists and whether the polarization can be efficiently used to control the stability of electron motion, e.g., the planes of attraction (nodes, antinodes).

A. Electric field polarized normally to $\vec{p}_0$

First we analyze the case whereby the SW is formed by two counterpropagating linearly polarized L beams with electric field perpendicular to the incident electron momentum, $\vec{p}_0 \equiv p_0 \hat{e}_x$. In this case electric and magnetic fields of the SW are $\vec{E}=E_{\mathrm{rel}} f(\xi)\hat{e}_\zeta \cos\eta \sin\tau$, $\vec{H}=-E_{\mathrm{rel}} f(\xi)\hat{e}_\xi \sin\eta \cos\tau$, where $\zeta=kz$. The Lorentz equations of motion (1) and (2) take the form

$$\frac{d\rho_\xi}{d\tau}=0, \quad \frac{d\rho_\eta}{d\tau}=-\frac{\rho_\zeta}{\gamma} f(\xi)\cos\tau \sin\eta, \tag{47}$$

$$\frac{d\rho_\zeta}{d\tau}=f(\xi)\left[\cos\eta \sin\tau+\frac{\rho_\eta}{\gamma}\sin\eta\cos\tau\right]. \tag{48}$$

Together with the standard kinematic equations

$$\frac{d\xi}{d\tau}=\frac{\rho_\xi}{\gamma}, \quad \frac{d\eta}{d\tau}=\frac{\rho_\eta}{\gamma}, \quad \frac{d\zeta}{d\tau}=\frac{\rho_\zeta}{\gamma}. \tag{49}$$

we have a complete system of differential equations for all three component (ξ,η,ζ) of coordinates and momenta. In the ξ direction we immediately have $\rho_\xi=\tilde{\rho}_\xi=\rho_0=\mathrm{const}$, $\tilde{\xi}=\beta_0\tau$. There are no fast oscillations of momentum in the ξ direction.

Similarly to Sec. III B we separate "slow" and "fast" electron motion and look for a solution in the form of Eqs. (31) and (33) and

$$\zeta \approx \tilde{\zeta}+\zeta^c\cos\tau+\zeta^s\sin\tau, \tag{50}$$

$$\rho_\zeta \approx \tilde{\rho}_\zeta+\rho_\zeta^c\cos\tau+\rho_\zeta^s\sin\tau. \tag{51}$$

The small parameters of the problem are μ_L and μ_ζ. The result for equation of "slow" motion is

$$\frac{d^2\tilde{\eta}}{d\tau^2}-\frac{f^2(\beta_0\tau)}{4\gamma_0^2}\sin(2\tilde{\eta})=0, \quad \tilde{\rho}_\eta=\gamma_0\frac{d\tilde{\eta}}{d\tau}, \tag{52}$$

$\tilde{\zeta}=0$, $\tilde{\rho}_\zeta=0$. Nonzero amplitudes of "fast" oscillations for the first harmonics in Eqs. (31), (33), (50), and (51) are

$$\rho_\zeta^c=-f(\beta_0\tau)\cos\tilde{\eta}, \quad \rho_\zeta^s=\frac{\tilde{\rho}_\eta}{\gamma_0}f(\beta_0\tau)\cos\tilde{\eta}, \tag{53}$$

$$\zeta^c=-\frac{\tilde{\rho}_\eta}{\gamma_0^2}f(\beta_0\tau)\cos\tilde{\eta}, \quad \zeta^s=-\frac{f(\beta_0\tau)}{\gamma_0}\cos\tilde{\eta}. \tag{54}$$

Equation of "slow" motion in the η direction (52) is again a pendulumlike equation. In contrast to the L beam with the E field parallel to $\vec{p}_0$, there is no relativistic reversal of stable and unstable planes of attraction. The equilibrium points of Eq. (52) are always the planes having zero electric field [$\eta=(n+1/2)\pi$], as in the nonrelativistic case. Comparison of the equations of motion (40) and (52) reveals that the transverse PF in both cases has the "regular" (nonrelativistic) component $f^2\sin(2\tilde{\eta})/4\gamma_0^3$ and the relativistic component $f^2\sin(2\tilde{\eta})\rho_0^2/4\gamma_0^3$. However, the relativistic component has different sign for different L-beam polarizations. In case when $\vec{E}\|\vec{p}_0$ (Sec. III B) the relativistic component of the PF

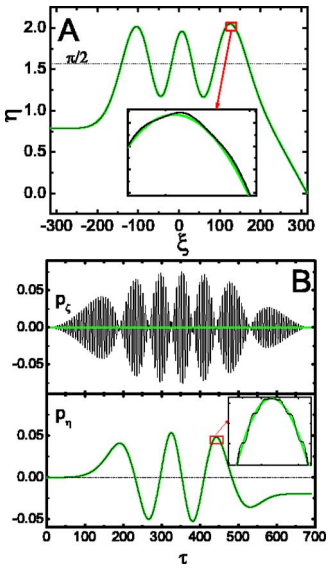

FIG. 10. (Color online) Trajectory (A) and momenta (B) of electron normally incident on a linearly polarized L beam with $\vec{E}\perp\vec{p}_0$ at $\eta_0=\pi/4$ with initial momentum $\rho_0=2.2$ ($f_{\rm pk}=0.2$, $\xi_L=200$).

pushes the particles toward the high E-field regions, whether when $\vec{E}\perp\vec{p}_0$ it repels electrons from the high field region together with the "regular" PF. Because of this, the PF in Eq. (52) is inversely proportional to γ_0, i.e., for $\gamma_0\gg 1$ it is much stronger than for the case of collinear configuration [see Eq. (40)], whereby the force is inversely proportional to γ_0^3.

Figure 10 demonstrates trajectory and momenta (ρ_ζ and ρ_η) of electron launched into a linearly polarized SW with the E field perpendicular to $\vec{p}_0$. Parameters of the simulation (except L-beam polarization) for this figure are the same as of Fig. 7 and we show the numerical solution of the full Lorentz equations (47) and (48) together with solution of the equation of "slow" motion (52). One can see, that in opposite to collinear configuration, even for $\rho_0>1$ electron still oscillates near the plane $\eta=\pi/2$ (E field is zero) and there is no relativistic reversal. Note, that the amplitudes of small oscillations in η and ρ_η are zero for the first harmonics. Corrections appear only in the second order in μ_L and μ_ξ. That is the reason why in Fig. 10 the "slow" variables $\tilde{\eta}$ and $\tilde{\rho}_\eta$ nearly coincide (within the linewidth) with η and ρ_η correspondingly. Small deviations are shown in the insets of the figure.

B. Circular polarization

Let us study now the case whereby the SW is formed by two counterpropagating circularly polarized L beams. One can distinguish two different situations: one is when the counterpropagating L beams have the same helicity (both are left/right circularly polarized), which we call the "counter-rotating" case, and another is when the L beams have different helicity (one is left- and another is right-circularly polarized), which we will call "corotating" case (the reason for this term is that an electron will experience rotating motion from both waves in the same direction). To carry out a meaningful comparison between results obtained for the SWs formed by linearly and circularly polarized L beams we chose the following field normalization: each L beam forming a SW is assumed to have the same intensity for all polarizations. With this normalization the amplitude of E and M fields of the circularly polarized L beams should be $\sqrt{2}$ times smaller than corresponding amplitude of the linearly polarized L beams studied in the previous sections. This way all the L beams that form SWs would have equal time-averaged energy flux (Poynting vector), and consequently, each SW would have the same time average of the energy density.

1. L beams with different helicity (corotating waves)

In the case when one L beam is left circularly polarized and another is right circularly polarized (i.e., at a given point E-field vectors of both L beams rotate in the same direction—corotating fields), the total electric and magnetic fields of the SW are $\vec{E}=E_{\rm rel}f(\xi)\cos\eta(\hat{e}_\xi\sin\tau+\hat{e}_\zeta\cos\tau)/\sqrt{2}$, $\vec{H}=E_{\rm rel}f(\xi)\sin\eta(\hat{e}_\xi\sin\tau+\hat{e}_\zeta\cos\tau)/\sqrt{2}$. The factor $1/\sqrt{2}$ is added to satisfy the normalization condition discussed above: namely, the SW studied here is formed by circularly polarized L beams of the same intensity as the linearly polarized L beams in Secs. III and IV A. Note, that in this case there is a "real" standing wave in the sense that one can distinguish nodes and antinodes of E and M fields as in the case of the SW formed by two linearly polarized L beams. That is, one can find points with a maximum E field and vanishing M field. This configuration can always be arranged by using a fully reflecting mirror as in the KD effect. The equations of motion in this case are

$$\frac{d\rho_\xi}{d\tau}=\frac{f(\xi)}{\sqrt{2}}\left[\cos\eta\sin\tau+\frac{\rho_\eta}{\gamma}\sin\eta\cos\tau\right],$$

$$\frac{d\rho_\eta}{d\tau}=\frac{f(\xi)\sin\eta}{\sqrt{2}\gamma}[-\rho_\xi\cos\tau+\rho_\zeta\sin\tau], \tag{55}$$

$$\frac{d\rho_\zeta}{d\tau}=\frac{f(\xi)}{\sqrt{2}}\left[\cos\eta\cos\tau-\frac{\rho_\eta}{\gamma}\sin\eta\sin\tau\right],$$

and the kinematic relations are given by Eq. (49). Using the same approach as before we separate "slow" and "fast" motion to obtain $\tilde{\rho}_\xi=\rho_0$, $\tilde{\rho}_\zeta=0$, the equation of "slow" motion

$$\frac{d^2\tilde{\eta}}{d\tau^2}-\frac{f^2(\beta_0\tau)}{4\gamma_0^4}\sin(2\tilde{\eta})=0,\quad \tilde{\rho}_\eta=\gamma_0\frac{d\tilde{\eta}}{d\tau}, \tag{56}$$

and the amplitudes of "fast" oscillations of momentum and coordinate for ξ and η components are given by Eqs. (34)–(37), where $f(\beta_0\tau)$ should be substituted by $f(\beta_0\tau)/\sqrt{2}$. For the ζ component we have

$$\rho_\zeta^s=\frac{f(\beta_0\tau)}{\sqrt{2}}\cos\tilde{\eta},\quad \rho_\zeta^c=-\frac{f(\beta_0\tau)}{\sqrt{2}\gamma_0}\tilde{\rho}_\eta\sin\tilde{\eta}, \tag{57}$$

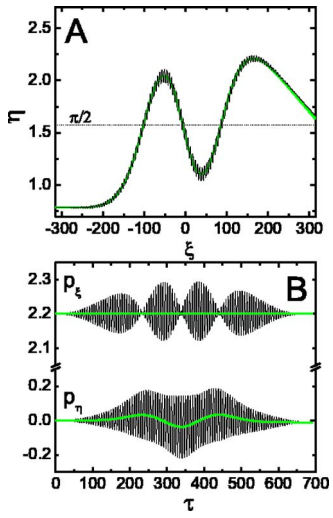

FIG. 11. (Color online) Trajectory (A) and momenta (B) of electron normally incident on a SW formed by two corotating L beams at $\eta_0=\pi/4$ with initial momentum $\rho_0=2.2$ ($f_{\rm pk}=0.28$, $\xi_L=200$).

$$\zeta^s=-\frac{f(\beta_0\tau)}{\sqrt{2}\gamma_0^2}\tilde{\rho}_\eta\sin\tilde{\eta},\quad \zeta^c=-\frac{f(\beta_0\tau)}{\sqrt{2}\gamma_0}\cos\tilde{\eta}. \tag{58}$$

Equation (56) is again a pendulumlike equation, which can easily be compared with the previously considered cases. Qualitatively, here again we have no reversal effect and the stable equilibrium points are the planes $\eta=(n+1/2)\pi$ (the planes where electric field vanishes), as in the case of linearly polarized SW with $\vec{E}\perp\vec{p}_0$. This result can be easily understood if we notice that the SW formed by corotating beams is a superposition of two $\pi/2$-phase shifted linearly polarized SWs with orthogonal polarizations: one has $\vec{E}\perp\vec{p}_0$ and the other has $\vec{E}\|\vec{p}_0$ (note, that in order to preserve the field normalization condition those two SWs should have amplitudes of the E and M fields reduced by a factor of $\sqrt{2}$). Then, using results for the PF for each polarization (Secs. III B and IV A) we can say that the SWs with $\vec{E}\|\vec{p}_0$ and $\vec{E}\perp\vec{p}_0$ have the PFs $\sim(1-\rho_0^2)/2$ and $\sim(1+\rho_0^2)/2$, respectively (the factor $1/2$ comes from the normalization). Adding those up one can see that the relativistic components of the PF cancel and the resultant PF is equal to the regular, nonrelativistic PF. This agrees with Eq. (56). Numerical simulations confirm analytical results (see Fig. 11 for $\rho_0>1$).

Although another relativistically-nonlinear effect, the generation of relativistic higher order harmonics, is a separate issue to be considered by us in detail for linearly polarized wave elsewhere, it is worth noting here that corotating circularly polarized SWs make an outstanding configuration for most efficient and broad spectrum generation of such harmonics. As was shown in Ref. [35], the number of harmonics for this configuration may go up as $\gamma_{\rm osc}^3$ (where $\gamma_{\rm osc}$ is the relativistic factor of fast oscillations/rotations of an electron), the same as in the cyclotron radiation, which is greater than for any other polarization configuration of a driving wave. At the same time, the total radiated power of these harmonics in corotating circularly polarized SWs is proportional to $\gamma_{\rm osc}^4$ when $\gamma_{\rm osc}\gg 1$ vs $\gamma_{\rm osc}^2$ for the linear polarization.

2. L beams of same helicity (counter-rotating waves)

The second case of the SW is when both L beams forming the SW have the same helicity (i.e., in a given point electric field vectors of two L beams rotate in opposite directions—counter-rotating beams, so that at any point the SW is linearly polarized, even though direction of the polarization changes from point to point). The fields in this configuration are $\vec{E}=E_{\rm rel}f(\xi)\sin\tau(\hat{e}_\xi\cos\eta+\hat{e}_\zeta\sin\eta)/\sqrt{2}$, $\vec{H}=E_{\rm rel}f(\xi)\cos\tau(\hat{e}_\xi\cos\eta+\hat{e}_\zeta\sin\eta)/\sqrt{2}$. Note, that in this wave $\vec{E}\|\vec{H}$ [36] and there are no nodes or antinodes of the E and M fields. At any point η the amplitude of square modulus of E-field vector is constant. Essentially, it is the case whereby there is no standing wave pattern of intensity and no transverse intensity gradient (compare with the SW in previous Sec. IV B 1). Let us choose the configuration in which at points $\eta=n\pi$ the SW is linearly polarized with $\vec{E}\|\vec{p}_0$, then at $\eta=\pi(n+1/2)$ the SW has $\vec{E}\perp\vec{p}_0$. The Lorentz equations of motion in this case are

$$\frac{d\rho_\xi}{d\tau}=\frac{f(\xi)}{\sqrt{2}}\left[\cos\eta\sin\tau+\frac{\rho_\eta}{\gamma}\sin\eta\cos\tau\right],$$

$$\frac{d\rho_\eta}{d\tau}=\frac{f(\xi)\cos\tau}{\sqrt{2}\gamma}[-\rho_\xi\sin\eta+\rho_\zeta\cos\eta], \tag{59}$$

$$\frac{d\rho_\zeta}{d\tau}=\frac{f(\xi)}{\sqrt{2}}\left[\sin\eta\sin\tau-\frac{\rho_\eta}{\gamma}\cos\eta\cos\tau\right],$$

together with the usual kinematic relations (49). The solution after the separation of slow and fast motion is $\tilde{\rho}_\xi=\rho_0$, $\tilde{\rho}_\zeta=0$, $\tilde{\xi}=\beta_0\tau$, the amplitudes of fast oscillations are given by Eqs. (34)–(37) [with $f(\beta_0\tau)$ substituted by $f(\beta_0\tau)/\sqrt{2}$ due to the normalization] for ξ and η components, and for the ζ component

$$\rho_\zeta^c=-\frac{f(\beta_0\tau)}{\sqrt{2}}\sin\tilde{\eta},\quad \rho_\zeta^s=-\frac{f(\beta_0\tau)}{\sqrt{2}\gamma_0}\tilde{\rho}_\eta\cos\tilde{\eta}, \tag{60}$$

$$\zeta^c=\frac{f(\beta_0\tau)}{\sqrt{2}\gamma_0^2}\tilde{\rho}_\eta\cos\tilde{\eta},\quad \zeta^s=-\frac{f(\beta_0\tau)}{\sqrt{2}\gamma_0}\sin\tilde{\eta}, \tag{61}$$

and for η component of momentum and coordinate we have

$$\frac{d^2\tilde{\eta}}{d\tau^2}+\frac{f^2(\beta_0\tau)}{4\gamma_0^4}\rho_0^2\sin(2\tilde{\eta})=0,\quad \tilde{\rho}_\eta=\gamma_0\frac{d\tilde{\eta}}{d\tau}. \tag{62}$$

Evidently, for this SW configuration stable equilibrium points are $\eta=n\pi$, where $\vec{E}\|\vec{p}_0$ and again, there is no reversal effect. Electrons are attracted to the planes with $\vec{E}\|\vec{p}_0$ at any value of p_0 (the case of $\rho_0<1$ is shown in Fig. 12). As explained in Sec. IV B 1, linearly polarized SW with $\vec{E}\|\vec{p}_0$ pushes the particles away from the regions of the E-filed maximum with the PF $\sim(1-\rho_0^2)/2$, whereas when $\vec{E}\perp\vec{p}_0$ the PF is $\sim(1+\rho_0^2)/2$. Subtracting these forces we obtain that the

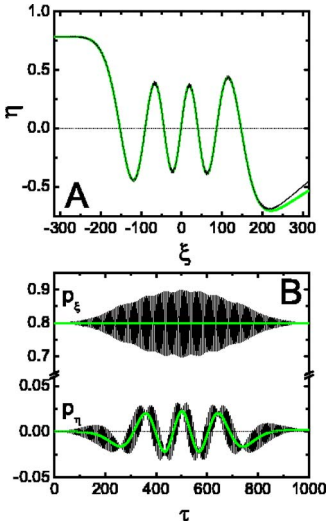

FIG. 12. (Color online) Trajectory (A) and momenta (B) of electron normally incident on a SW formed by two counter-rotating L beams at $\eta_0=\pi/4$ with initial momentum $p_0=0.8$ ($f_{\mathrm{pk}}=0.14$, $\xi_L=200$).

net force is $\sim\rho_0^2$ and the equilibrium planes of the SW are the planes with $\vec{E}\|\vec{p}_0$ [as predicted by Eq. (62)]. Another way to understand this result is to remember that this counter-rotating SW has an unusual property, namely, in this wave $\vec{E}\|\vec{H}$ [36]. Then it follows, that in the planes where $\vec{E}\|\vec{p}_0$ we have $\vec{p}_0\times\vec{H}=0$ and there is no nonrelativistic contribution to the PF that repels the particle away from these planes. This is a quite remarkable result, because even though the SW has a constant intensity of the electric field, and, in this sense, there is no transverse gradient, electrons still "feel" the difference between the planes of the SW via relativistic component of the transverse PF.

V. CONCLUSION

The ponderomotive force as it is known in non-relativistic case, gets transformed into much richer set of spatial relativistic interactions. We have developed the relativistic analytical theory of electron motion in a standing wave of ultrapowerful laser having various polarizations. Our major result is that for certain polarizations the PF normal to the incident momentum, $\vec{p}_0$ reverses its sign as the momentum exceeds relativistic scale, which makes high-intensity areas (antinodes) attracting instead of expected low-intensity areas (nodes). Optimal configuration to observe relativistic reversal is collinear electron-SW configuration, whereby electric field is linearly polarized and parallel to the initial momentum of electron. The reversal effect is absent in the cases of circularly polarized L beams and when electric field of laser is normal to $\vec{p}_0$. However, changing mutual helicity of the circularly polarized beams one can control the stability planes of electron motion in the SW. Counter-rotating standing wave has homogeneous intensity profile along the axis of propagation and does not have a field gradient in that direction; however, electrons are attracted to the planes with $\vec{E}\|\vec{p}_0$. We also found an adiabatic invariant and reflection-transmission threshold energy of electrons for antinode modes, "sneaky" modes in the nodes, and large Kapitza-Dirac effect in transmission and reflection. Our numerical simulations confirmed the analytical results.

ACKNOWLEDGMENTS

We are grateful to Peter Shkolnikov for fruitful discussions. This work was supported by AFOSR.

[1] A. E. Kaplan and A. L. Pokrovsky, Phys. Rev. Lett. **95**, 053601 (2005).
[2] H. A. H. Boot and R. B. R.-S. Harvie, Nature (London) **180**, 1187 (1957).
[3] A. V. Gaponov and M. A. Miller, Sov. Phys. JETP **7**, 168 (1958).
[4] T. W. B. Kibble, Phys. Rev. Lett. **16**, 1054 (1966).
[5] F. A. Hopf, P. Meystre, M. O. Scully, and W. H. Louisell, Phys. Rev. Lett. **37**, 1342 (1976).
[6] M. V. Fedorov, *Interaction of Intense Laser Light With Free Electrons*, Vol. 13 of *Laser Science and Technology* (Harwood Academic Publishers, Chur, Switzerland, 1991).
[7] L. D. Landau and E. M. Lifshitz, *Mechanics* (Butterworth-Heinemann, Oxford, 2003).
[8] A. Ashkin, Phys. Rev. Lett. **24**, 156 (1970).
[9] T. W. Hänsch and A. L. Schawlow, Opt. Commun. **13**, 68 (1975).
[10] *Laser Manipulation of Atoms and Ions*, edited by E. Arimondo, W. D. Phillips, and S. Strumina (North Holland, Amsterdam, 1992).
[11] G. Grynberg and C. Robilliard, Phys. Rep. **355**, 335 (2001).
[12] R. R. Freeman, P. H. Bucksbaum, H. Milchberg, S. Darack, D. Schumacher, and M. E. Geusic, Phys. Rev. Lett. **59**, 1092 (1987).
[13] E. Wells, I. Ben-Itzhak, and R. R. Jones, Phys. Rev. Lett. **93**, 023001 (2004).
[14] P. L. Kapitza and P. A. M. Dirac, Proc. Cambridge Philos. Soc. **29**, 297 (1933).
[15] M. V. Fedorov, Opt. Commun. **12**, 205 (1974).
[16] P. H. Bucksbaum, D. W. Schumacher, and M. Bashkansky, Phys. Rev. Lett. **61**, 1182 (1988).
[17] D. L. Frelmund, K. Aflatoonl, and H. Batelaan, Nature (London) **413**, 142 (2001).
[18] C. Gahn, G. D. Tsakiris, A. Pukhov, J. Meyer-ter-Vehn, G. Pretzler, P. Thirolf, D. Habs, and K. J. Witte, Phys. Rev. Lett. **83**, 4772 (1999).
[19] J. Faure, Y. Glinec, A. Pukhov, S. Kiselev, S. Gordienko, E. Lefebvre, J.-P. Rousseau, F. Burgy, and V. Malka, Nature (London) **431**, 541 (2004).
[20] A. E. Kaplan, Phys. Rev. Lett. **48**, 138 (1982).
[21] G. Gabrielse, H. Dehmelt, and W. Kells, Phys. Rev. Lett. **54**, 537 (1985).

[22] A. E. Kaplan, Phys. Rev. Lett. **56**, 456 (1986).
[23] A. E. Kaplan and Y. J. Ding, IEEE J. Quantum Electron. **24**, 1470 (1988).
[24] C. S. Weimer, F. L. Moore, and D. J. Wineland, Phys. Rev. Lett. **70**, 2553 (1993).
[25] E. Yablonovitch, N. Bloembergen, and J. J. Wynne, Phys. Rev. B **3**, 2060 (1971).
[26] E. S. Sarachik and G. T. Shappert, Phys. Rev. D **1**, 2738 (1970).
[27] J. N. Bardsley, B. M. Penetrante, and M. H. Mittleman, Phys. Rev. A **40**, 3823 (1989).
[28] F. V. Hartemann, S. N. Fochs, G. P. Le Sage, N. C. Luhmann, J. Woodworth, M. D. Perry, Y. J. Chen, and A. K. Kerman, Phys. Rev. E **51**, 4833 (1995).
[29] Y. I. Salamin and F. H. M. Faisal, Phys. Rev. A **55**, 3678 (1997).
[30] J. L. Chaloupka and D. D. Meyerhofer, Phys. Rev. Lett. **83**, 4538 (1999).
[31] D. Bauer, P. Mulser, and W.-H. Steeb, Phys. Rev. Lett. **75**, 4622 (1995).
[32] Z.-M. Sheng, K. Mima, J. Zhang, and J. Meyer-ter-Vehn, Phys. Rev. E **69**, 016407 (2004).
[33] B. Liesfeld, J. Bernhardt, K.-U. Amthor, H. Schwoerer, and R. Sauerbrey, Appl. Phys. Lett. **86**, 161107 (2005).
[34] I. S. Gradsteyn and I. M. Ryzhik, *Table of Integrals, Series, and Products*, 5th ed. (Academic Press, Boston, 1994).
[35] A. E. Kaplan and P. L. Shkolnikov, Phys. Rev. Lett. **88**, 074801 (2002).
[36] C. Chu and T. Ohkawa, Phys. Rev. Lett. **48**, 837 (1982).